OPEN ACCESS
IOP Publishing
Superconductor Science and Technology
Supercond. Sci. Technol. **33** (2020) 054004 (7pp)
https://doi.org/10.1088/1361-6668/ab7fbd

Future Circular Collider beam screen: progress on Tl-1223 HTS coating

A Leveratto[1], A Saba[1,2], S Holleis[3], M Himmerlich[4], B Henrist[4], S Fernandez-Peña[4], A Moros[5], J Bernardi[5], M Eisterer[3], C Bernini[1], R Vaglio[1,6], M Putti[2], C Ferdeghini[1], S Calatroni[4] and E Bellingeri[1]

[1] CNR-SPIN, I-16152, Genoa, Italy
[2] University of Genova, Physics Department, I-16126, Genoa, Italy
[3] Atominstitut, TU Wien, Stadionallee 2, A-1020, Vienna, Austria
[4] CERN, European Organization for Nuclear Research, 1211 Geneva 23, Switzerland
[5] University Service Centre for Transmission Electron Microscopy (USTEM), TU Wien, Vienna, Austria
[6] University of Naples Federico II and INFN, Physics Department, I-80125, Naples, Italy

E-mail: alessandro.leveratto@spin.cnr.it

Received 5 November 2019, revised 2 March 2020
Accepted for publication 13 March 2020
Published 6 April 2020

Abstract

Thallium-1223, a superconductor with high critical temperature ($T_c \sim 120$ K) and high irreversibility line is a promising alternative to copper layers as a low surface impedance material in particle accelerator components. In the existing design of the Future Circular Collider (FCC-hh), for reasons of cryogenic efficiency and vacuum stability, the beam screen that shields the dipoles from synchrotron radiation has to stay at best in the temperature range between 40 and 60 K, in which copper surface resistance might be too high to prevent beam instabilities due to wakefields. This paper reports the progress on the realization of thallium-1223 based high temperature superconducting (HTS) coatings realized by electrochemical deposition. The study of the Tl-1223 phase has been carried out on precursor-pellets and films. Transport characterization revealing a very high irreversibility line and also high local critical currents obtained from Scanning Hall Probe Microscopy (SHPM) measurements will be shown. A first analysis of compatibility in vacuum has been carried out and the generation of secondary electrons (SEY) has been investigated as well.

The encouraging results, although not conclusive, will state that thallium-based phase could be suitable for the proposed application.

Keywords: Tl-1223, thallium, high temperature superconductors, Future Circular Collider

(Some figures may appear in colour only in the online journal)

1. Introduction

A conceptual design for the next generation of a circular collider at CERN (Future Circular Collider, FCC) was recently presented [1–3]. Many aspects of the final configuration are under investigation and the challenge to substitute the standard copper coating in the beam screen with high temperature superconductors (HTS) [4] is still open. As already discussed in [5], the choice falls only on RE-123 and Tl-1223 [6], progress on REBCO tapes can be found in [7]. Frequency and field intensity limits as well as the possible issue of a thermal runaway have already been discussed [8, 9]. The coating with Tl-1223 has the peculiarity to be realized via electrochemical deposition [10, 11] thanks to the high out-of-stoichiometry-tolerance with respect to RE-123. Furthermore, it is a cheap and scalable technique, which could be considered for a direct deposition on tubes or arbitrarily shaped templates. Here we report on the work conducted by showing the interesting properties that this phase holds through the characterization

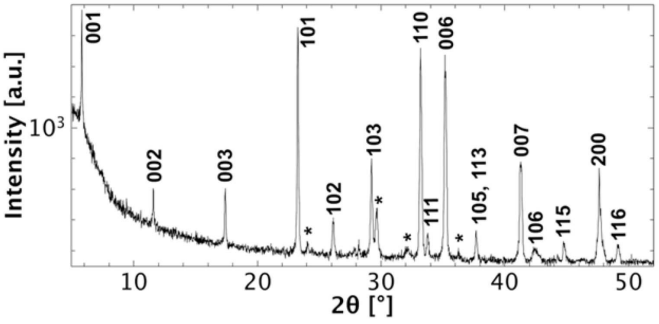

Figure 1. X-ray diffractogram of a precursor-pellet. A quite pure Tl-1223 phase has been observed [6], contributions from complex oxides' peaks are indicated with *.

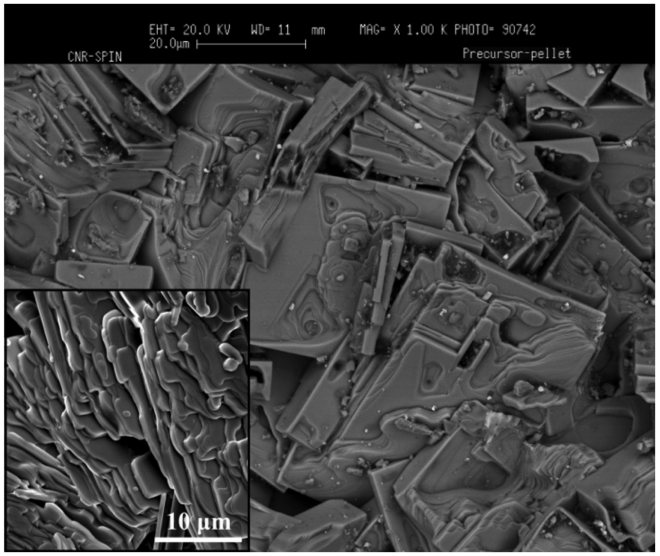

Figure 2. The main image shows a SEM measurement (detection of backscattered electrons) which evidences the sample homogeneity, ascribed to the Tl-1223 phase. In the inset the plate-like Tl-1223 grains morphology are clearly visible.

of coatings and precursor-bulks, useful for the film growth, by means of electrical resistance as a function of temperature and magnetic field, R(T, B), and scanning Hall probe microscopy (SHPM). Measurements for general understanding and to verify if thallium-based HTS are suitable for the beam chamber have been carried out performing vacuum and secondary electron generation tests. The study on the bulk led up to obtain the 8-elements stoichiometry necessary for our application in order to carry on the coating realization with an already optimised element ratio. Further the precursor-bulks are employed during the high temperature heat treatment.

2. Experimental

2.1. Sample preparation: bulk and film

A detailed description of the samples realization, in form of bulk and coating, is given below. Since bulks, as anticipated above, will be involved in the heat treatment process for the phase growth on coatings, have been labelled as precursor-pellets or -bulks.

2.1.1. Bulk preparation. The synthesis consists in the realization of a complex oxide compound based on Tl, Bi, Pb, Ba, Sr, Ca, and Cu with the desired stoichiometric ratio through carbonates and oxides in the form of powder. In our case, for reasons of the required properties for the foreseen application, we selected $Tl_{0.7}Bi_{0.2}Pb_{0.2}Sr_{1.6}Ba_{0.4}Ca_{1.9}Cu_3O_{9+x}$. Two 24 h long calcinations, involving $SrCO_3$, $BaCO_3$, $CaCO_3$, and CuO, have been performed at 900 °C in pure O_2 flux and at 980 °C in air. Subsequently PbO and Bi_2O_3 were added and after 1–3 h grinding with a vibratory micro mill in air the powder has been dried and subjected to 60 h planetary ball milling in argon. The last step is the addition of Tl_2O_3 mixed in Agate mortar under very safe conditions. Pellets of 20 mm diameter, 2 mm thick pressed in air at 200 bar are reacted for 3 h in oxygen flux at 905 °C. An almost pure Tl-1223 phase has been obtained as shown in the x-ray diffractogram (Bragg-Brentano geometry, Panalytical X'Pert PRO) and in the Scanning Electron Micrograph (SEM), respectively in figures 1 and 2.

2.1.2. Electrochemical deposition. The films are realized by electrochemical deposition in a 3-electrode system on suitable substrates: silver [12] and strontium titanate (STO, $SrTiO_3$) intentionally metallized via sputtering; a flat cell is employed. The working, counter and reference electrodes are the chosen substrate, platinum grid, and $Ag/AgNO_3$ 0.1 M in Dimethyl Sulfoxide (DMSO, Sigma-Aldrich, 99.9%, anhydrous, sure-sealed grade), respectively. Nitrates have been dissolved in 250 ml of DMSO. Due to the large difference in the overpotential for the different ions, the stoichiometry of the solution is very far from the one required on the substrate. By iterative analysis of deposited precursors with energy dispersive x-ray spectroscopy (EDX) we obtained the element contents required as follows: 0.25 g $TlNO_3$, 0.18 g $Bi(NO_3)_3 \cdot 5H_2O$, 0.18 g $PbNO_3$, 2.73 g $Sr(NO_3)_2$, 1.52 g $Ba(NO_3)_2$, 1.63 g $CaNO_3 \cdot H_2O$ and 1.33 g $Cu(NO_3)_2 \cdot H_2O$. Typically the film deposition is performed between −2.9 V and −3.1 V for 600 s with a commercial potentiostat. With DMSO being a high boiling point solvent, the samples are dried in vacuum at 120 °C before performing the final high temperature heat treatment.

The samples are processed in a three-zone tube furnace in a partially closed system inside a gold foil crucible for 10 min at 885 °C. Since thallium oxide is volatile above 710 °C it is mandatory to keep the sample in a thallium atmosphere. To overcome this restriction Tl_2O_3 powder (4 mg) and Tl-1223 pellets are used. The main scope is to find the best compensation between losses and reabsorption of thallium-bismuth-lead and since the precursor-pellet releases with an already balanced stoichiometry helps the growth of Tl-1223 phase. As shown in the inset of figure 3, a certain degree of texturing can be observed from the rocking curve of the Tl-1223 (002) peak, tentatively evidenced by the arrows in figure 4. However, the control of the thallium atmosphere is still in phase of optimisation. SEM-EDX analysis, shown in figure 5, reveals that the

plate-like grains do not achieve uniform coverage of the substrate yet and evidences that the transformation of the precursors into the desired phase is not complete, since the Tl-1212 phase and complex oxides are detected as well. In this condition, it seems that Tl-1212 grains preferentially grow on top of Tl-1223 grains (it is visible in figure 5 that the blue phase grows on the top of the green one).

2.2. Electrical transport and magnetization measurements

Precursor-pellets and coatings were evaluated by different methods. Precursor-pellets, holding a sufficient grain connection, could show a superconducting transition in the electrical resistivity and the critical temperature has been analysed as a function of the applied magnetic field. On the contrary, thin films on Ag and STO substrates were characterized by means of SQUID (superconducting quantum interference device) magnetometry and Scanning Hall Probe Microscopy

2.2.1. Characterization of precursor-pellets. The resistance behaviour in magnetic fields up to 9 T is shown in figure 6. The shift of the zero state caused by the applied field gives the estimate of the irreverisibility and the upper critical fields, H_{irr} and H_{c2}, (figure 7) adopting the 10% R_N and 90% R_N method, where R_N is the normal state resistance. The measurements have been performed by a Quantum Design PPMS.

The extrapolation shows a very high H_{c2} and, more importantly, a very high H_{irr}. Compared to literature we obtained one of the highest values reported [13, 14]. An estimation of the H_{irr} dependence for higher fields is inserted as dashed line in figure 7 confirming the suitability of Tl-1223 for the FCC-hh environment.

2.2.2. Characterization of films. The superconducting transition temperature was determined by AC susceptibility measurements with amplitude of 30 μT and a frequency of 1 Hz in a SQUID magnetometer (MPMS, Quantum Design). The measurement of a thin film on Ag substrate, as seen in figure 8, reveals two transitions. The first, with $T_{c,onset} = 107$ K, can be attributed to the Tl-1223 phase, while the second transition with $T_{c,onset} = 75$ K shows the contribution of the Tl-1212 phase. The high T_c of the Tl-1223 is promising; with further optimisation of the heat treatment, a better phase purity is expected.

The remnant field profiles were mapped with a Hall scanner in an 8 T cryostat setup with micrometer resolution. Everything but a round spot of superconducting film was etched off the Ag substrate with hydrochloric acid in order to fit into the SHPM setup. An image obtained with a digital microscope (VHX-6000, Keyence) is given in figure 9(a), the dark spots indicate the superconducting areas. The sample was cooled to 5 K in zero field and then magnetized with 1.5 T. The area scan shows many individual grains and grain clusters with high trapped field, indicated by bright colours, as can be seen in figure 9(b). The optical image and magnetic field map can be directly compared, and an overlay of the two images shows a perfect agreement, seen in figure 9(c). In order to get a better insight into the currents within single grains and across grain boundaries, a high-resolution scan of a smaller area was performed. Figure 9(d) shows the trapped field of a few grain clusters, which amounts to 60 mT. By inversion of Biot-Savart's law, the spatial distribution of J_c can be calculated from the measured trapped field [15]. The white arrows in figure 9(e) show the direction of current flow in grains and across grain boundaries for the measured grain clusters. The average magnitude of the critical current density in these grain clusters amounts to $J_c = 8 \times 10^{10}$ Am^{-2} at 5 K.

The same experiments were also performed on a thin film on STO substrate.

The resulting area scan, which is given in figure 10(a), shows the trapped field of a larger grain cluster. In this case, the maximum trapped field amounts to 100 mT at 5 K. Calculation of the J_c distribution gives the same value as on the Ag substrate on a larger area, see figure 10(b).

The microstrucure of the measured thin film on STO substrate was further investigated by means of SEM (FEI Quanta 200 FEGSEM) and TEM (FEI TECNAI F20) imaging. Through precise comparison of SEM images and magnetic maps, the areas with the highest trapped fields can be identified. For such an area the overlay of magnetic map and SEM image is given in figure 11(a). With a focused ion beam (FEI Quanta 200 3D DB-FIB), two TEM lamellas were prepared from this sample, one lamella taken from an area with high trapped field and one from an area with no trapped field, as indicated by the arrows leading from figures 11(a) to (b). In this process, a protective Platinum layer is deposited on the sample surface, the lamella is cut out and the thickness of the lamella is reduced to about 100 nm. In the area with high trapped field, the TEM image shows one large grain with a thickness of 1.8 μm flat on the substrate surface, seen in figure 11(c). With EDX analysis, the different areas can be identified: on the top, we find the Pt protective layer, next, a thin layer of SiO, which stems from small contaminations in the fabrication process, and then a large Tl-1223 grain on top of the STO substrate. We find the same compositions in the lamella taken from the area with no trapped field, shown in figure 11(d). In this case however, we find multiple Tl-1223 grains, randomly oriented on the substrate surface. This underlines the necessity for grain orientation, as the current flow is blocked by the misalignment of the Tl-1223 grains.

2.3. Vacuum and secondary electron yield behaviour

Coating the beam screen mandates compliance with certain requirements inherent of the particle accelerator environment. For example, the vacuum base pressure must not be deteriorated by outgassing from the layer, and the secondary electron generation probability of the top material should be low enough to avoid formation of an electron cloud during circulation of the proton beam in order to avoid beam instabilities and excessive heat load to the cryogenic system [16–18]. Thallium compounds, and in particular Tl-1223, have never been used in particle accelerators, leaving a lack of knowledge in literature about its intrinsic properties concerning any possible release

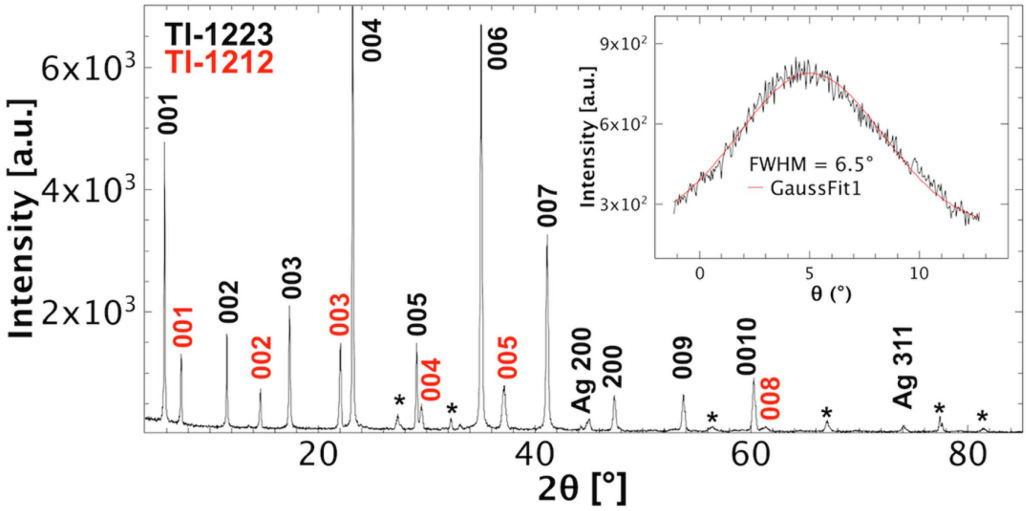

Figure 3. X-ray diffractogram of a thallium-based HTS coating. Phases and orientation are shown in black for Tl-1223 and in red for Tl-1212 [6]. The inset shows the rocking curve of the Tl-1223 (002) peak.

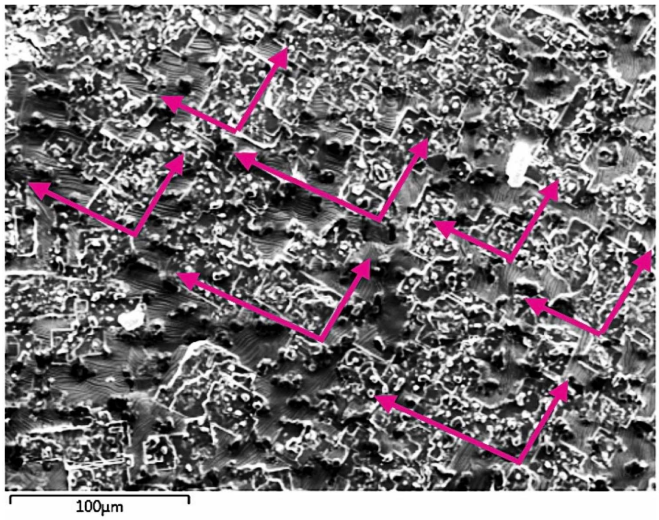

Figure 4. SEM image of an electrodeposited sample after heat treatment. The arrows are guides to visualize the in plane texturing.

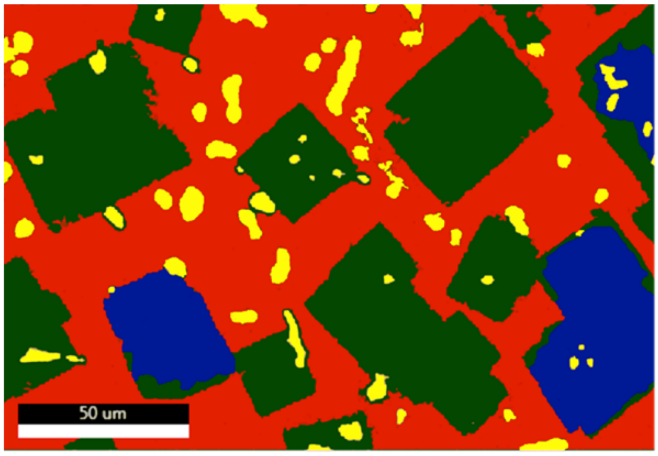

Figure 5. SEM-EDX analysis. In the colour map Tl-1223 (Green), Tl-1212 (Blue), Ca,Pb-O (Yellow), and Silver (Red) have been identified.

of gaseous species in vacuum, or the secondary electron yield (SEY) of this material. In this section we discuss outgassing and residual gas analysis (RGA) measurements, and a first x-ray photoelectron spectroscopy (XPS) and SEY analysis performed on precursor-pellets.

One precursor-pellet was placed onto an aluminium foil for a standard vacuum characterization measurement. The specific H_2O outgassing rate after 10 h of pumping was 2×10^{-7} mbar l^{-1} s^{-1} cm^{-2}, ~500 times the reference for unbaked, clean copper surfaces. The vacuum pump-down exhibited a linear behaviour in logarithmic time/total pressure scale, with a slope very close to −1, indicating open porosities responsible for the large outgassing rate. The RGA after 24 h of pumping was readily within CERN's acceptance criteria for unbaked components [19], except for a rather pronounced O_2 release and some F contamination, the latter barely exceeding the acceptance criteria probably due to packaging. In addition, XPS analysis of the aluminium foil itself revealed that no high atomic mass elements (Tl, Pb, Bi) are released by the pellet.

XPS analysis was performed on the surface of one pellet. The surface composition indicates a heavily oxidized surface with more than 50 at.% of oxygen due to air exposure. The surface carbon content is ~15 at.%, showing a rather clean surface, in good correlation with the RGA analysis. Tl, Pb and Bi appear to exist in a single oxidation state, while the constituents Ca, Sr and Ba exhibit different chemical states due to their high surface reactivity.

The SEY δ is the ratio between the number of generated secondary electrons per single electron impinging on a surface. It can be measured in lab experiments using a tuneable electron source considering $\delta = I_\delta / I_i$, where I_δ is the total emission current and I_i is the current of the incident electron beam [20]. In the present Large Hadron Collider (LHC) configuration

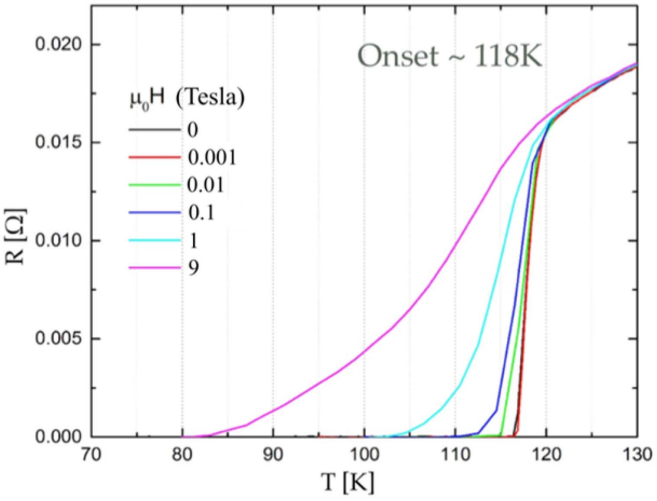

Figure 6. 4-probe resistance measurement on varying the temperature at different applied magnetic fields as reported in the *legenda* by different colours.

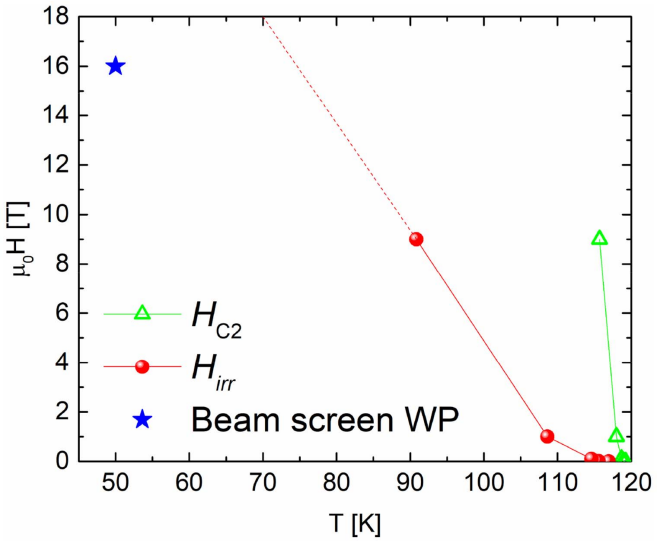

Figure 7. Extrapolation from graph in figure 6 of the upper critical (green) and irreversibility (red) magnetic field The dashed red line is a prediction at high field showing that we are well above the ideal FCC-beam screen working point (16 T, 50 K) indicated with the blue star.

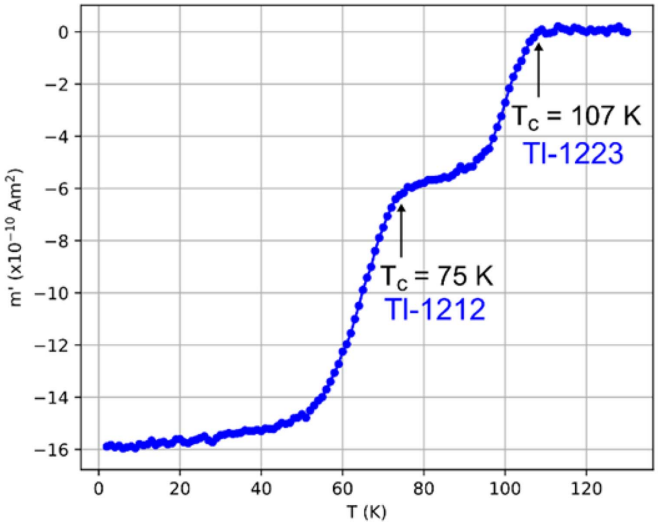

Figure 8. AC susceptibility of thin film on Ag substrate. Two transitions are identified at approximately 107 K and 75 K, which correspond to the Tl-1223 and Tl-1212 phase, respectively.

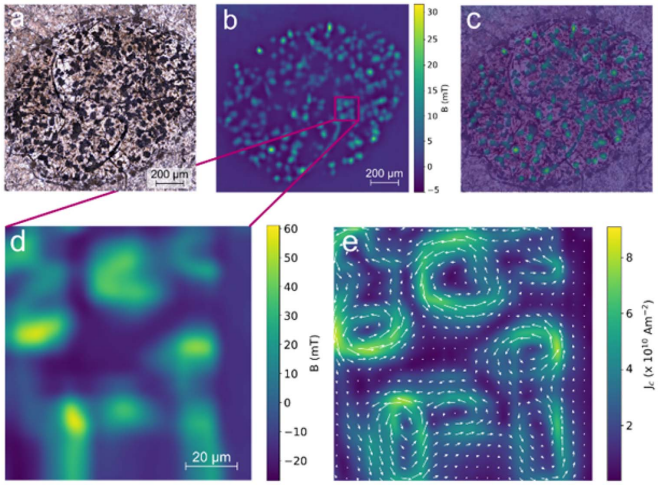

Figure 9. Image of grains on Ag substrate (a), and corresponding area scan of the trapped field (b). An overlay of the two images (c) shows perfect agreement between optical image and the magnetic measurement. High resolution scan of a smaller area (d), and corresponding critical current density distribution (e).

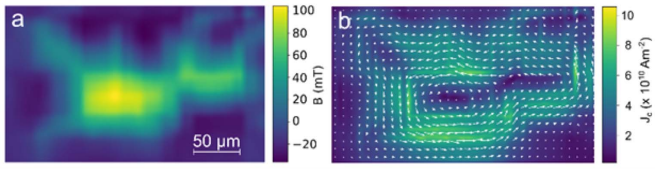

Figure 10. Trapped field of the Tl-1223 grain cluster on STO substrate (a), and corresponding critical current density distribution (b).

at CERN, the inner beam screen copper surface exhibits a maximum SEY below 1.3 after beam scrubbing/conditioning 250 eV electrons [20, 21].

The beam screen of the FCC has similar SEY requirements as the LHC beam screen. For Tl-1223, the SEY coefficient was determined within this study for precursor-pellets with different surface topography. Figure 12 includes the dependency of the SEY on the primary electron energy for the bare Tl-1223 surfaces. The SEY maximum is between 2.05 and 2.25 for all investigated samples, while the curve distribution depends on the surface roughness.

The surface of one selected pellet (#1) was modified by an amorphous carbon (a-C) coating utilizing DC magnetron sputtering according to a procedure described in detail in [7]. First a 150 nm thick Ti buffer layer was deposited followed

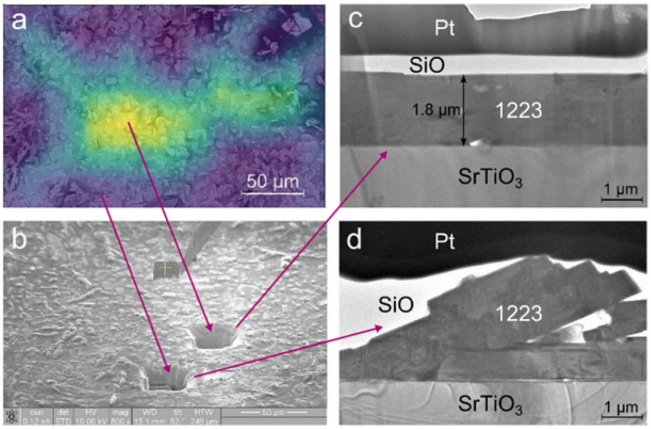

Figure 11. Overlay of trapped field and SEM image of a thin film on STO substrate (a), and preparation of two TEM lamellas with a Focused Ion Beam (b). TEM images of areas with high trapped field (c) and no trapped field (d) show the desired Tl-1223 phase with good and bad grain alignment, respectively.

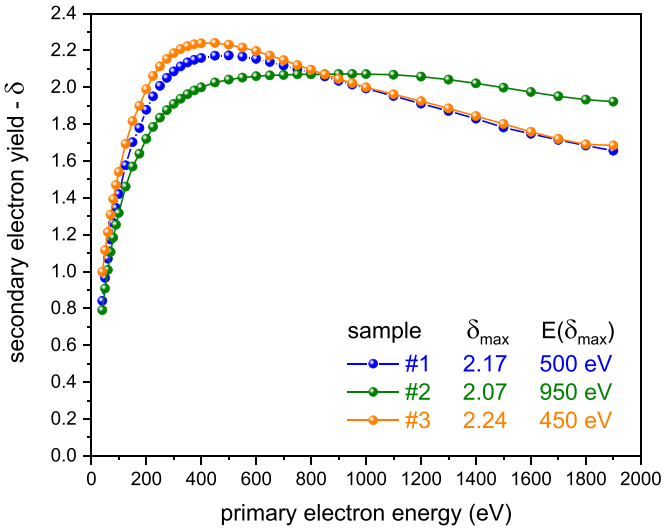

Figure 12. Secondary electron yield curves of bare Tl-1223 surfaces as a function of primary electron (PE) energy.

by addition of a 100 nm thick a-C top layer. A comparison of the SEY curves before and after coating is shown in figure 13, revealing that the SEY maximum (δ_{max}) has considerably dropped to 0.77, exhibiting the typical SEY energy dependence of a-C coatings (δ_{max} at 250 eV).

Consequently, the bare Tl-1223 surface has a rather high initial δ_{max} at room temperature. Nevertheless, the application of a thin amorphous carbon coating on top of the superconducting layer reduces this value to below unity, which is a very promising result for further development of this approach. It was recently demonstrated that such a coating on commercial REBCO tapes can also reduce the maximum SEY from initially ∼3 to a value close to 1.2 [7]. The lower value in the present study could be due to the different surface topography of the investigated samples.

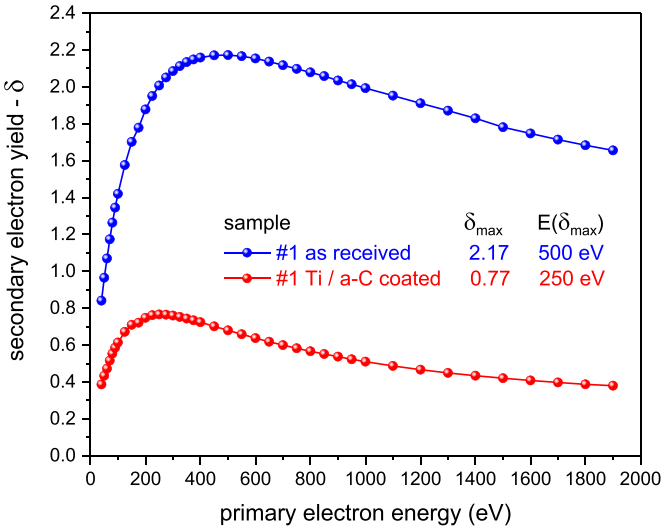

Figure 13. Secondary electron yield of a Tl-1223 pellet in dependence of primary electron (PE) energy before and after Ti/a-C coating.

3. Conclusion

In this work, we presented the progress on development of Tl-1223 HTS coatings for future implementation as low impedance layers on particle accelerator components, specifically the FCC-hh beam screen. We described in detail the optimised synthesis and sample preparation of electrodeposited films and of precursor-pellets, which are useful for the high temperature heat treatment of the coatings. For bulk samples, we extrapolated a very high irreversibility line, while for Tl-1223 coatings, large plate-like grains have been obtained on silver and STO substrates, even if a fully superconducting coverage is still not achieved. A quite high critical current density of $J_c \sim 8 \times 10^{10}$ Am^{-2} at 5 K in self-field was calculated from SHPM measurements. Tl-1223 is found to be applicable in vacuum environments, and with an additional amorphous carbon top coating, it exhibits a remarkably low coefficient of secondary electron generation ($\delta_{max} = 0.77$), making it compatible with accelerator environments. In light of the results obtained, we can affirm, even though there are critical issues mainly due to the volatility of thallium, that the Tl-1223 phase can respond well to the requirements desired for this kind of application.

Acknowledgments

The work has been supported by CERN Funding Addendum FCC-GOV-CC-0049 (EDMS1580502, KE3112) within the FCC study, and the Marie Sklodowska-Curie Training Network EASITrain (European Advanced Superconductivity Innovation and Training), funded by the European Union's H2020 Framework Programme under grant agreement no. 764879. The authors would like to acknowledge the help of Mauro Taborelli (CERN) for coordinating the SEY analyses, Guillaume Rosaz (CERN) for coordinating the a-C coatings

and Andrea Malagoli (CNR-SPIN) for fruitful discussions about the samples heat treatment.

ORCID iDs

A Leveratto https://orcid.org/0000-0001-8480-2884
M Eisterer https://orcid.org/0000-0002-7160-7331
M Putti https://orcid.org/0000-0002-4529-1708
S Calatroni https://orcid.org/0000-0002-2769-8029

References

[1] Collaboration F C C Abada A *et al* 2019 *Eur. Phys. J.* C **79** 474
[2] Tomás R *et al* 2016 *Nucl. Part. Phys. Proc.*, **273** 149
[3] Tavian L J 2014 *Cryogenics Future Circular Collider Study Kickoff Meeting* (Switzerland: University of Geneva) (availabe at: http://indico.cern.ch/event/282344/contributions/1630775) (accessed 12–15 February)
[4] Calatroni S 2016 *IEEE Trans. Appl. Supercond.* **26** 35002
[5] Calatroni S, Bellingeri E, Ferdeghini C, Putti M, Vaglio R, Baumgartner T and Eisterer M 2017 *Supercond. Sci. Technol.* **30** 075002
[6] Bellingeri E and Flükiger R 2002 *Handbook of Superconducting Materials, Institute of Physics Publishing*, ed D Cardwell and D Ginley (Cambridge: University of Cambridge, NREL)
[7] Puig T *et al* 2019 *Supercond. Sci. Technol.* **32** 094006
[8] Calatroni S and Vaglio R 2017 *IEEE Trans. Appl. Supercond.* **27** 3500506
[9] Vaglio R and Calatroni S 2019 *Eur. Phys. J. Spec. Top.* **228** 749–54
[10] Bellingeri E, Suo H L, Genoud J Y, Schindl M, Walker E and Flukiger R 2001 *IEEE Trans. Appl. Supercond.* **11** 3122
[11] Jeong D Y, Kim Y H, Shirage P M, Kim S Y, Horiuchi S and Lee J H 2007 *Supercond. Sci. Technol.* **20** 1239
[12] Genoud J L, Suo H L, Schindl M, Bellingeri E, Tybell T, Walker E and Flukiger R 2001 *IEEE Trans. Appl. Supercond.* **11** 3371
[13] Zheng D N, Campbell A M, Liu R S and Edwards P P 1993 *Cryogenics* **33** 46
[14] D N Z, J D J, A R J, A M C, W Y L, Doi T, Okada M and Higashyama K 1995 *J. App. Phys.* **77** 5287
[15] Hengstberger F, Eisterer M, Zehetmayer M and Weber H W 2009 *Supercond. Sci. Technol.* **22** 025011
[16] Chao A W 1993 *Physics of Collective Beam Instabilities in High Energy Accelerators* (Weinheim: Wiley-VCH)
[17] Baglin V, Bojko J, Grobner O, Henrist B, Hilleret N, Scheuerlin C and Taborelli M 2000 *Proceedings of EPAC 2000 (Vienna, Austria)* pp. 217–221 (http://accelconf.web.cern.ch/AccelConf/ e00/PAPERS/THXF102.pdf)
[18] Jimenez J M, Arduini G, Collier P, Ferioli G, Henrist B Hillert N, *et al* 2003 CERN LHC Project Report 634 1 (https://cds.cern.ch/record/615159)
[19] Lecercle A, Mongelluzzo A, Somoza Ferreira J A, Michet A and Chiggiato P 2014 Procédure d'acceptation de composants pour les systèmes à vide des injecteurs non étuvés du LHC CERN (https://edms.cern.ch/document/1437531/1)
[20] Petit V, Taborelli M, Neupert H, Chiggiato P and Belhaj M 2019 *Phys. Rev. Accel. Beams* **22** 083101
[21] Larciprete R, Grosso D R, Commisso M, Flammini R and Cimino R 2013 *Phys. Rev. Accel. Beams* **16** 011002